Strain-induced instability of spherical nanodiamond hydrocarbons: Effect of surface CH_n and charging

Mehdi Heidari Saani,[1,2,*] Tayebeh Ghodselahi,[3,4] and Keivan Esfarjani[5]
[1]*Semiconductor Component Industry, 19575-199 Tehran, Iran*
[2]*Physics Group, Maleke Ashtar University, 83145-115 Shahin Shahr, Iran*
[3]*Department of Physics, Sharif University of Technology, 11365-9161 Tehran, Iran*
[4]*Institute for Studies in Theoretical Physics and Mathematics, 19395-5531, Tehran, Iran*
[5]*Department of Physics, University of California–Santa Cruz, California 95064, USA*
(Received 6 March 2008; revised manuscript received 19 September 2008; published 24 March 2009)

The structural stability and vibrational properties of different sizes and charge states of the hydrogen saturated spherical and cagelike C nanoparticles were investigated by means of *ab initio* density-functional theory. The cagelike nanoparticles remain stable and stiff under structural relaxation, whereas specific sizes and charge states of spherical C nanoparticles deform dramatically and dissociate under the relaxation. In order to see the possibility of observation this effect in other semiconductor nanoparticles, two smallest sizes of spherical Si nanoparticles were also examined and similar instabilities were obtained. We explain the induced large amount of positive strain of unstable spherical C and Si nanoparticles by the presence of CH_3 and SiH_3 terminations on the surface. These terminations result in a very packed arrangement of polar C-H bonds and consequently a large value of Coulombic potential on the surface and corresponding strain in the volume of the clusters, respectively. We demonstrate that the variation in formation and electronic properties with size correlate with the variation in CH/CH_2+CH_3 ratio of the surface with size in agreement with the recently reported empirical correlation suggested by x-ray absorption spectroscopy measurements. Likewise, we discuss the reported empirical correlation between H coverage and strain in porous Si and some other corresponding experimental evidences in porous Si. The calculation of the vibrational properties supports the reported structural instabilities.

DOI: 10.1103/PhysRevB.79.125429 PACS number(s): 61.46.Hk, 61.46.Bc

I. INTRODUCTION

Atomic arrangement and composition of surface in addition to the quantum confinement have been suggested as the main factors governing the physical properties of semiconductor nanoparticles.[1] Quantum confinement causes the material's optical gap to widen. The larger optical gap prompts dramatic changes in electronic and optical properties. Nanoparticles are also different from bulk in that the percentage of atoms at or near their surface is far greater. The surface of nanoparticles thus plays an important role in determining the particle's electronic and optical properties.[2]

In the era of technological applications of nanostructured materials, attention was originally focused on semiconductor nanoparticles constructed from Si[3] or Ge,[4] as they can easily be integrated with existing Si fabrication techniques. Although silicon is an indirect band-gap semiconductor and thus a poor optoelectronic material, Si nanoparticles show an intense room-temperature photoluminescence[5] (PL) and electroluminescence[6] due to the quantum confinement effect. The breakthrough in isolating H-terminated diamondoids has sparked interest in measuring and calculating their structural and optoelectronic properties.[7–10] The effect of attachment of different atoms to the surface of the Si nanoparticles on the electronic highest occupied molecular orbital (HOMO) - lowest unoccupied molecular orbital (LUMO) energy gap has been reported by Buttard *et al.*[11] They empirically discussed the surface stress and also its induced bulk strain and deformation based on the effect of H desorption from the surface of porous Si by annealing. We have already reported a strong correlation between the ratio of the bulk C atoms to the surface H atoms (C/H) with the formation energy and HOMO-LUMO energy gap.[12] Recently x-ray absorption spectroscopy (XAS) measurements have revealed an empirical correlation between electronic structure of the nanodiamond particles with the surface CH/CH_2 ratio.[13]

In this paper, we explain the origin of the calculated structural instability and softness in specific sizes and geometries of spherical nanodiamond particles. In order to examine the occurrence of such instabilities in other semiconductor nanoparticles, we have also investigated the structural stability of two smallest spherical Si nanoparticles where more experimental evidences are available. We will be investigating two types of diamond nanoparticles, which we will call "spherical" and "cagelike." The former structure is obtained by taking one carbon atom as the center of the sphere and including all the neighboring carbon atoms in the diamond structure within some radius R, and finally terminating all remaining dangling bonds by H. The latter consists in juxtaposing cages of adamantane C_{10} near each other. After introductory section, we explain the calculation method in Sec. II. In Sec. III, we will explain the calculation results and show that the geometry and arrangement of C-H bonds on the surface due to different compositions of CH, CH_2, and CH_3 terminations cause different surface potentials and consequently different structural strain, deformation, and vibronic properties for C and small Si nanoparticles, even though the formation energies of these nanoparticles are comparable. We discuss the effect of charging on the induced surface potential in nanoparticles. The reported empirical correlation between varia-

TABLE I. The strain ($\Delta a/a$) of different sizes of spherical C and Si nanoparticles in their different charge states. S and U in parentheses represent the stable and unstable structures of the clusters after relaxation, respectively.

Cluster Charge state	C_5H_{12}	$C_{17}H_{36}$	$C_{29}H_{36}$	$C_{35}H_{36}$	$C_{47}H_{60}$	Si_5H_{12}	$Si_{17}H_{36}$
Particle size (nm)	0.43	0.68	0.73	0.85	0.93	0.44	1.0
Neutral	0.6 (S)	– (U)	3.2 (S)	1.9 (S)	8.4 (U)	2.6 (S)	6 (U)
Negative	0.6 (S)	– (U)	3.7 (S)	1.9 (S)	8.4 (U)	– (U)	– (U)
Positive	– (U)	– (U)	3.2 (S)	9 (S)[a]	– (U)	6 (U)	4 (U)

[a]In the positive state of $C_{35}H_{36}$, the value of strain is due to the only one broken bond between central C atom and one of its four neighbors.

tions in electronic properties with surface CH/CH_2+CH_3 ratio of different nanoparticle sizes will be discussed. We also explain the reported[13] empirical correlation between H coverage and surface induced strain in PS. Finally in Sec. IV, we summarize the results.

II. THEORY AND METHODS

We employed *ab initio* density-functional theory (DFT) cluster method to calculate structural and vibronic properties of H-terminated C and Si particles in their different charge states. In order to investigate the effect of atomic geometry and surface C-H arrangement on stability, cagelike and spherical nanodiamond particles were considered. We also examined two smallest sizes spherical Si_5H_{12} and $Si_{17}H_{36}$ nanoparticles. A perfect geometry relaxation for the nanoparticles without symmetry constraints was performed until the root mean square of Cartesian forces on each atom reduces below 5 meV/Å. The GAUSSIAN03 code was used for self-consistent density-functional calculations.[14] Due to the small atomic number of carbon, we performed an all electron calculation. Atomic centered 6–31G extended basis set for C was used in this study. For the Si atoms we used core effective potentials CEP-31G. We have also examined the extended diffusive basis set 6-31++G for this calculation and similar results emerged. The calculated total energies converged to within 10^{-5} a.u. The B3LYP (Ref. 15) three-parameter hybrid exchange functional was employed.

The formation energy of nanoparticles was calculated from the calculated total energies in the DFT framework,[9]

$$E_f(C_mH_n) = \frac{E(C_mH_n) - mE(C) - (n/2)E(H_2)}{m}.$$

In this relation $E(C_mH_n)$, $E(C)$, and $E(H_2)$ are the total energies of the C_mH_n nanoparticle, C atom, and H_2 molecule, respectively.

III. RESULTS AND DISCUSSIONS

In Sec. III A, we will discuss strain calculation results in different C and Si nanoparticles and distinguish the stable and unstable nanoparticles. Then we will discuss the origin of instability for specific sizes of spherical particles based on surface potential. In Sec. III B we explain the mechanical stability, softness, and vibrational spectra for the C and Si nanoprticles to support the instability results of spherical nanoparticles in Sec. III A based on vibrational spectra and softness of nanoparticles. Finally in Sec. III C we will discuss the reported correlation between electronic structure and surface $CH/(CH_2+CH_3)$ ratio and other related reported experimental evidences on PS.

A. Effect of coordination and charging on strain and structural stability

After performing structural relaxations we found that all cagelike nanodiamond particles conserve their ideal diamond structures and bond lengths. There is however an appreciable positive strain for spherical C and Si nanoparticles. For some specific sizes and charge states, the spherical C and Si nanoparticles dissociate after atomic relaxation. The strain of each nanoparticle was calculated from $\Delta a/a$ formula, where a is the average bond length of related C-C and Si-Si bonds in the C and Si nanoparticles and Δa is the difference between these average bond lengths and related bulk bond lengths. Results for spherical C and Si nanoparticles have been summarized in Table I.

In Table I, we have also listed the stable and unstable structures of spherical C and Si nanoparticles in different charge states. We define the unstable structures as structures that dissociate after atomic relaxation.

In Fig. 1, the size-dependent instability of spherical nanodiamond particles after atomic relaxation has been shown. All unstable nanoparticles in Fig. 1, have been dissociated from their central region. In other words the bonds between central atoms and their neighbors have been broken. This is in agreement with the reported results concerning accumulation of the strain in the central region of the spherical C, Si, and Ge nanoparticles.[16,17] However to the best of our knowledge, no dissociation has been reported in the literature so far. In order to understand the origin of the instability of these specific sizes of C nanoparticles, we have listed in Table II the number of C atoms which have four neighboring C atoms, for different nanoparticles, and also the number of surface C atoms which are bonded to H via CH, CH_2, and CH_3 terminations. The numbers of SiH, SiH_2, and SiH_3 terminations for Si nanoparticles are the same as those listed in Table II for C particles.

From Table II, we see that in the unstable $C_{17}H_{36}$ and $C_{47}H_{36}$ nanoparticles, we have 12 CH_3 terminations on the surface, whereas CH_3 is absent on the surface of the stable

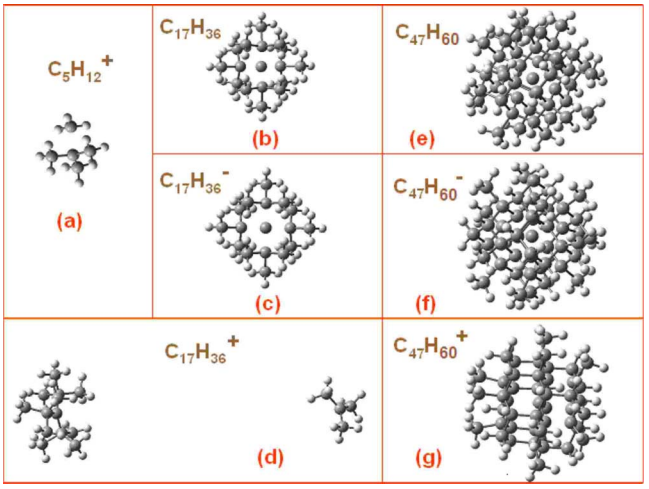

FIG. 1. (Color online) Unstable structure of spherical C nanoparticles with different charge state after atomic relaxation.

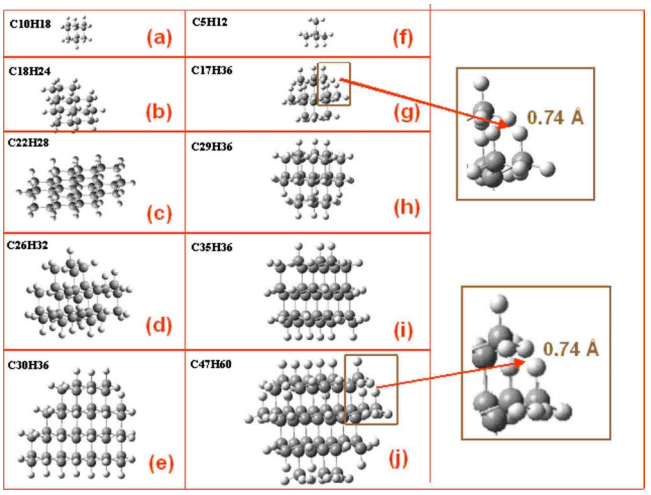

FIG. 2. (Color online) Initial structures of the [(a)–(e)] cagelike and [(f)–(j)] spherical nanodiamond particles. The presence of CH_3 on the surface of the spherical C_5H_{12}, $C_{17}H_{36}$, and $C_{47}H_{60}$ spherical particles results in a 0.74 Å distance between neighboring protons ($H^{\delta+}$) in two adjacent CH_3.

$C_{29}H_{36}$ and $C_{35}H_{36}$ nanoparticles. It is interesting to note that similar to the stable spherical nanoparticles, all sizes of cagelike nanodiamond particles that remain stable after atomic relaxation do not have any CH_3 termination on their surfaces. For the $C_{17}H_{36}$ nanoparticle, we observe the maximum amount of strain. For this nanoparticle there are only CH_3 terminations on the surface in contrast to other nanoparticles that are listed in Table I.

In order to interpret the relationship between unstability and presence of the CH_3 termination on the surface, we take a look at the initial unrelaxed structure of the unstable spherical nanodiamond particles in Fig. 2. As it has been shown in Fig. 2, in such spherical particles, the presence of CH_3 termination increases the density of directional CH bonds on the surface of these spherical nanodiamonds. This causes a very small distance between two protons or partially polar H atoms ($H^{\delta+}$) in two adjacent CH_3, which is about 0.74 Å comparable with 0.7 Å, the bond length of H_2 molecule. For comparison, this small distance is smaller than the C-H bond length, 1.09 Å. At this small distance, there is large Columbic repulsion between adjacent protons and consequently a considerable potential and tension on the surface.

TABLE II. Number of bulk and surface atoms of each nanodiamond particle with their related atomic environment.

Cluster		Bulk	Surface		
Cagelike	Spherical	C	CH	CH_2	CH_3
$C_{10}H_{18}$		0	4	6	0
$C_{18}H_{24}$		1	10	7	0
$C_{22}H_{28}$		2	12	8	0
$C_{26}H_{32}$		3	14	9	0
	C_5H_{12}	1	0	0	4
	$C_{17}H_{36}$	5	0	0	12
	$C_{29}H_{36}$	5	12	12	0
	$C_{35}H_{36}$	5	24	6	0
	$C_{47}H_{60}$	17	12	6	12

Due to presence of the CH_3 terminations on the surface of the $C_{17}H_{36}$ and $C_{47}H_{36}$ nanoparticles and corresponding large electrostatic potential on the surface, there is a large amount of local strain (see Table I) in these clusters that breaks some C-C bonds in the central region of these particles. In contrast to positively charge states, in the neutral and negatively charged C_5H_{12} nanoparticle, the accumulated strain only deforms the nanoparticle. This effect can be attributed to further enhanced (positive) surface potential by positive charging of nanoparticles.

We have also examined the structural stability of the smallest spherical Si nanoparticles, i.e., Si_5H_{12} and $Si_{17}H_{36}$. Similar to C nanoparticles, there are SiH_3 terminations on the surface, in addition to the SiH and SiH_2 terminations. In Table I, we also reported the stability condition of different charge states of two sizes of Si nanoparticles after atomic relaxation. From this table the neutral charge state of the Si_5H_{12} is stable in agreement with previous *ab initio* calculation results.[16]

The results of the relaxed structure of Si nanoparticles are also shown in Fig. 3. As one can see in Fig. 3 and Table I, for the Si_5H_{12} nanoparticle, we observed instability after a full relaxation in both positive and negative charge states and also in all charge states of $Si_{17}H_{36}$. In these two sizes of nanoparticles, the smallest distance between the two protons on the surface is 1.35 Å that is smaller than the Si-H bond length, 1.5 Å. We suggest that this small distance results in a large amount of surface potential and induces bulk strain that deforms the structure of the neutral state of Si_5H_{12} and dissociates all charge states of $Si_{17}H_{36}$ that has been terminated only by SiH_3, similar to their C counterpart.

From Table I, we observe that the probability of finding unstable structures for charged states of Si and C particles after atomic relaxation is larger than the related probability for neutral particles. We attribute this effect to the localization of the extra charge after ionization on the surface of the particles. This is due to the electrostatic repulsion between

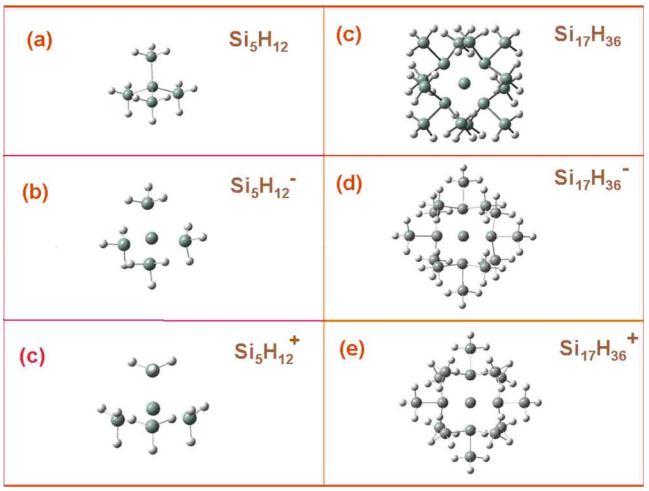

FIG. 3. (Color online) Relaxed structures of different charge states of spherical Si_5H_{12} and $Si_{17}H_{36}$ nanoparticles.

extra charges that pushes the charge toward the surface of the nanoparticles. A similar conclusion was obtained by direct charge distribution analysis of HOMO-LUMO molecular orbitals of charged nanoparticles. We show in Fig. 4 the isocharge surface of single electron HOMO and LUMO states for spherical C_5H_{12} and Si_5H_{12} nanoparticles in their neutral and charged states.

From Fig. 4, one can realize that for C nanoparticles, in the HOMO states, there is a considerable probability of finding electrons inside the nanoparticles especially on the bonds between C atoms. However, in the LUMO state, the isocharge surfaces of the nanoparticles are delocalized and mostly have been extended to the outer part of the nanoparticle, in agreement with previous *ab initio* results.[10] For the C nanoparticle, the surface H atoms are screened significantly by electronic charge cloud in HOMO and LUMO states whereas, for the Si nanoparticle, there is a smaller degree of screening of the surface H atoms in the HOMO and LUMO states.

The redistribution of the surface charge of the ionized particles results in relaxation and rearrangement of surface atoms and C-H bonds. The surface-atom rearrangement can alter the distance between partially positive H atoms on the surface resulting in a larger electrostatic repulsion and surface potential. This causes a large amount of bulk strain in H-terminated nanoparticles. The variation in strain of Si nanocrystal with thermal annealing was reported by Buttard *et al.*[11] They attributed the induced variation in the bulk strain and also the surface stress to the variation in the H coverage due the H desorption by annealing. Kim *et al.*[18] proposed that the decrease in strain upon thermal annealing in vacuum is a result of the desorption of physisorbed gas molecule from the native oxide of the pore walls in the PS layer.[19] Our calculated +2%–+4% strain for elastically stiff spherical nanoparticles in Table I is larger than measurement results by Buttard *et al.*[11] who obtained less than 1% positive induced strain.

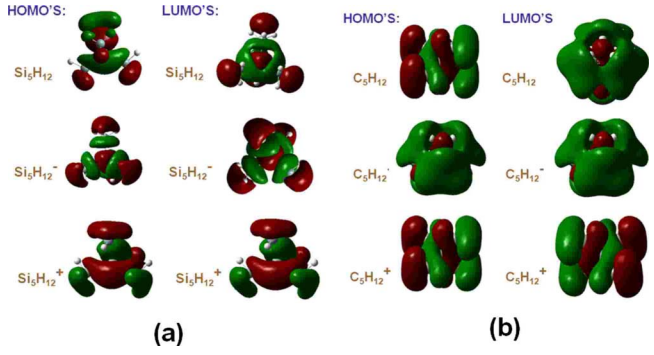

FIG. 4. (Color online) The isocharge surface of the HUMO and LUMO for different charge states of the spherical (a) Si_5H_{12} and (b) C_5H_{12} nanoparticles.

Our obtained positive strain for H terminated particles is in agreement with Sugiyama-Nittono[19] explanation concerning the expansion of lattice due to the H coverage. The lattice parameter of porous Si increases with the growth of an oxide layer. At room temperature, this has been observed for the growth of native oxide and of anodic oxide.[20] Ito *et al.*[21] proposed that the decrease in the strain upon annealing in vacuum is related to the desorption in chemisorbed hydrogen from Si atoms in the pores and the increase in strain is related to the formation of Si-H bonding during anodization. Our proposed picture for the microscopic origin of the surface potential supports the above experimental evidences.

Li and Vanderbilt[22] performed an *ab initio* DFT calculation for the surface of Si(111):H and obtained a very small stress for this surface. By considering their result for an infinite surface, our obtained large amount of the strain for the small H covered nanoparticles may be due the large curvature of these nanoparticles. This suggestion is in agreement with the observed increase in the strain with decreasing pore size in porous Si and in the presence of native oxide.[23,24]

B. Mechanical stability and vibrational spectra

The vibrational spectrum of a molecule or a cluster is intimately related to its intrinsic structure.[9] Such calculation can be used to estimate the mechanical stability of the nanostructures that determines the stability of the nanoparticles under deformation. The mechanical stability is different from theromodynamic stability that only considers the heat of formation of a nanoparticle and determines the abundance of the nanoparticle.

Here, we calculate the vibrational frequencies of the investigated sizes of H-terminated C and Si nanoparticles in order to trace any difference between vibronic properties of the stable and unstable structures of nanoparticles. We should be able to compare vibrational results with results in Sec. III A concerning the very soft structure of some specific sizes of spherical C and Si nanoparticles.

Similar to previously reported calculation,[9] we could not find any imaginary frequencies for cagelike C nanoparticles, implying that all of the calculated isomers of nanodiamond particles are stable or metastable. Anyhow our atomic relaxation results in Sec. III A have determined the stable, metastable, and unstable structures of C and Si particles. The smallest vibrational modes of different sizes and charge states of the cagelike nanodiamond particles are summarized in Table III.

TABLE III. List of the smallest vibrational modes of the cagelike (Nos. 1–4), spherical (Nos. 5–11) C, and spherical (Nos. 12–17) Si nanoparticles with the related IR intensities and structural stability condition.

No	Cluster	Charge state	Stability	Smallest frequency (cm^{-1})	IR intensity
1	$C_{10}H_{18}$	Neutral	S	802.53	0.42
2	$C_{18}H_{24}$	Neutral	S	704.62	0.7
3	$C_{22}H_{28}$	Neutral	S	436.25	0.15
4	$C_{26}H_{37}$	Neutral	S	483.51	0.22
5	C_5H_{12}	Neutral	S	934.42	0.70
6	C_5H_{12}	Negative	S	440.97	10.20
7	C_5H_{12}	Positive	U	213.62	0.18
8	$C_{17}H_{36}$	Neutral	U	130.06	2.15
9	$C_{29}H_{36}$	Neutral	S	377.73	1.77
10	$C_{29}H_{36}$	Negative	S	416.91	4.55
11	$C_{35}H_{36}$	Neutral	S	350.96	0.15
12	Si_5H_{12}	Neutral	S	106.83	3.51
13	Si_5H_{12}	Negative	U	−330.09	260.05
14	Si_5H_{12}	Positive	U	33.97	15.26
15	$Si_{17}H_{36}$	Neutral	U	101.1	0.41
16	$Si_{17}H_{36}$	Negative	U	−86.47	16.91
17	$Si_{17}H_{36}$	Positive	U	−176.76	86.38

"S" and "U" represent the stable and unstable structures after relaxation, respectively. From Table III, the structures of all sizes of cagelike nanodiamond particles (No. 1 to No. 4) with different charge states are stable after atomic relaxation. By increasing the cluster size, the lowest vibrational modes of cagelike nanodiamond particles vary from 802.53 to 483.51 cm^{-1}; this means that all sizes of these nanoparticles remain elastically stiff in agreement with structure relaxation results in Sec. III A that obtained bond lengths about 1.54 Å after relaxation in the absence of CH_3 terminations. In any case, by increasing the cluster size the C nanoparticles become mechanically softer due to the reduced effect of quantum confinement.

In Table III from No. 5 to 11, we have listed the smallest vibrational modes of different charge states of spherical C nanoparticles with their structural stability condition after atomic relaxation (see Fig. 1). The vibrational frequency of the stable structures decreases from the 934.42 cm^{-1} for the smallest particle C_5H_{12} to the 350.96 cm^{-1} for the largest stable $C_{35}H_{36}$ nanoparticles. The lowest vibrational frequency of the unstable structures, i.e., positively charged C_5H_{12} and neutral $C_{17}H_{36}$ particles are 213.62 cm^{-1} and 130.06 cm^{-1}, respectively. The smallest frequencies of the stable particles are comparable with calculated frequencies of the cagelike structures in Table III. Therefore the smallest vibrational frequencies of stable structures are much larger than that of unstable ones. We conclude that, from the vibronic property point of view, unstable nanoparticles in previous sections that undergo a large amount of induced strain become dramatically softer than stable ones.

In Table III from No. 12 to No. 17, we have listed the smallest vibrational modes of the different sizes and charge states of spherical Si nanoparticles. The only stable structure after relaxation is the neutral Si_5H_{12} nanoparticle. The smallest vibrational frequencies of the unstable Si nanoparticles vary from −330.09 up to 101.1 cm^{-1}. We observe a clear enhancement of the softness by charging spherical Si nanoparticles. The smallest vibrational frequencies of some unstable structures are negative in contrast to the positive vibrational frequencies of the stable C nanoparticles. These negative frequencies imply an absolute structural instability for these nanoparticles.

A measure of relative softness would be to compare the smallest vibrational frequency with $\pi c/d$ where d is the nanoparticle size and c is the smallest speed of sound in the bulk material. To obtain the vibrational frequency of a cluster, knowing the phonon spectrum of the bulk phase, due to the finite-size effect, the wave vector only takes the allowed quantized wave number $n\pi/\mathrm{d}$ where n is an integer number. Therefore the smallest phonon frequency should be comparable to $\pi c/d$ where C in diamond and Si are 12 km/s and 4.7 km/s, respectively.

From Table IV, the smallest vibrational frequencies of absolutely stable $C_{29}H_{36}$ and $C_{35}H_{36}$ spherical C nanoparticles are larger than their smallest acoustic phonon frequency ($\pi c/d$), reflecting quantum confinement effects. On the other hand, the acoustic phonon frequencies of unstable or metastable (too soft spherical nanoparticles), i.e., $C_{17}H_{36}$, Si_5H_{12}, and $Si_{17}H_{36}$, are larger than their corresponding smallest vibrational frequencies. Dolino *et al.*[25] discussed the effect of the adsorption and wetting phenomena of the surface on the elastic softening in porous Si by x-ray-diffraction observation in order to explain the magnitude of the observed strains. They concluded that softening of the elastic constants characteristic of porous materials enhances the magnitude of these deformations. Comparing smallest vibra-

TABLE IV. Size, stability condition, smallest acoustic phonon frequency, and smallest vibrational frequency of some C and Si nanoparticles. In the stability row the S, U, and S* respectively mean stable, unstable, and too soft structures after relaxation.

Nanoparticle	C_5H_{12}	$C_{17}H_{36}$	$C_{35}H_{36}$	Si_5H_{12}	$Si_{17}H_{36}$
Stability	S	U	S	S*	S*
Diameter (Å)	4.30	6.814	8.47	6.25	10.20
$\pi c/d$	465.55	921.63	236.12	124.8	76.47
Smallest vibrational frequency (cm^{-1})	802.53	130.06	350.96	106.83	40.63

tional modes of C and Si nanoparticles, after renormalization by their bulk speed of sound in Table IV, we conclude that charging has a more significant effect on the softness of Si nanoparticles than their C counterparts.

In conclusion, provided that there is structural stability, the abundance would depend on the formation energies and charging will soften the nanoparticles. The smallest vibrational frequencies of the C and Si nanoparticles scale almost as the inverse of their size. The vibrational frequencies of the strain-induced particles are appreciably smaller than frequencies of nanoparticles that do not undergo any strain. Furthermore, Si nanoparticles are mechanically softer than their C counterparts.

C. Correlation between electronic structure and surface $CH/(CH_2+CH_3)$ ratio

In Fig. 5, we have shown the dependence of the energy gap on the relaxation of the surface H atoms in the original direction of the Si-H bonds of the unrelaxed surface. The inset of Fig. 5 shows the variation in the formation energy with the Si-H bond length. The formation energy of nanoparticle reaches a minimum value around 1.5 Å in agreement with the equilibrium distance of the Si-H bond in SiH_4. For this bond length, the value of the energy gap is 5.52 eV.

We observe a very strong dependence of the energy gap on Si-H bond length in Fig. 5, where the energy gap varies from 5.6 eV to 4.9 eV for Si-H bond lengths in the range of 0.18–1.3 Å. From this figure we conclude that the arrangement and relaxation of the surface H atoms that alter surface potential cause a very significant variation in the electronic and optical properties of Si nanoparticles. The strong size-dependent PL spectra of semiconductor nanoparticles indicate that the observed PL originates from the recombination of electron-hole pairs confined in nanoparticles and consequently depends on the energy gap.[26,27]

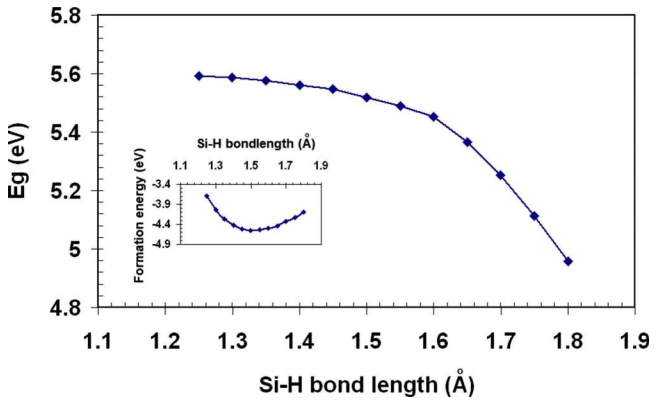

FIG. 5. (Color online) Electronic energy gap versus the surface Si-H bond length which determines the surface potential. The variation in the formation energy versus the surface Si-H bond length is also shown in the inset.

Larre *et al.*[28] found that both the refractive index and the optical absorption of the PS and H desorption has been also represented by Halimaoui *et al.*[29] There is controversial interpretation about the effect of the surface stress on PL. Friedersdorf *et al.*[30] proposed that oxidation stress can shift the PL energy. However a direct measurement of PL shift under hydrostatic pressure gives more complex results. According to the measurements of the shift of the indirect gap of bulk Si due to pressure,[31,32] the oxidation stresses are not large enough to produce the observed shifts of the PL energy.[33] X-ray-diffraction experiments[34] show that the associated stress due to wetting by a liquid is small and could not be at the origin of the quenching of the photoluminescence when the PS is in presence of an organic vapor or liquid. Wolkin *et al.*[35] and Vasiliev *et al.*[36] reported a theoretical model based on quantum confinement and surface passivation, which explains the experimental results concerning the shift of PL due to H passivation or after exposure to oxygen. From our *ab initio* results in Fig. 5, it seems that induced surface potential in porous Si due to Si-H bond relaxation could be at the origin of the drastic variations in the optical properties produced by anodic oxidation or vapor adsorption due to altering composition, arrangement, and the morphology of the surface. After demonstrating the essential role of the presence of CH_3 termination on the structural stability of nanodiamond particles, we investigate the effect of the relative numbers of surface CH, CH_2, and CH_3 terminations on the HOMO-LUMO energy gap of nanodiamond particles. In Fig. 6, we have shown the variation in the CH/CH_2+CH_3 ratio with the nanoparticle size for cagelike and spherical nanodiamond particles and also in the inset of this figure we have shown the variation in the HOMO-LUMO energy gap of the cagelike and spherical particles with the size.[12] In Fig. 6, for the cagelike nanodiamond particles there is a monotonic increase in the ratio of CH/CH_2+CH_3 with size whereas the variation in this ratio for spherical particles is not monotonic and has a maximum value for $C_{35}H_{36}$. As the inset of Fig. 6 shows, the monotonic and nonmonotonic variations in the CH/CH_2+CH_3 ratio are in very good agreement with the reported[12] variation in the HOMO-LUMO energy gap of the cagelike and spherical nanodiamond particles

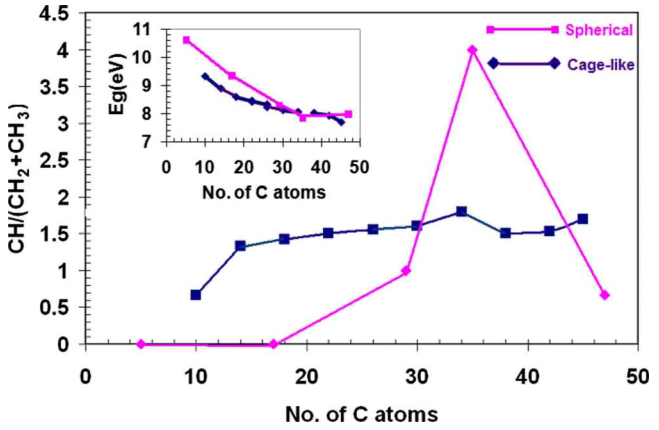

FIG. 6. (Color online) The variation in CH/CH_2+CH_3 ratio with size for different sizes of the cagelike and spherical nanodiamond particles. In the inset the variation in HOMO-LUMO energy gap with the number of the C atoms of the cagelike and spherical nanodiamond particles has been shown from Ref. 12.

with the size as it has been shown in the insets of Fig. 6. From Ref. 12 we know that for the cagelike C particles, the formation energy increases and HOMO-LUMO energy gap decreases monotonically in agreement with monotonic variation in CH/CH_2+CH_3 ratio with the size. For the spherical C particles, the variation in formation energy and HOMO-LUMO energy gap with size reach a maximum and a minimum, respectively,[12] in agreement with nonmonotonic variation in CH/CH_2+CH_3 ratio with the size. For spherical particles HOMO-LUMO energy gap and CH/CH_2+CH_3 ratio reach their extreme values for $C_{35}H_{36}$. These correlations can be explained with the relation between polar character of C-C bonds in clusters with relative number of different terminations.

The *ab initio* results of Fig. 6 support the recently reported[13] experimental work on the XAS (x-ray photoelectron spectroscopy) measurement on nanodiamond particles. Wielley *et al.*[13] empirically found a nearly direct linear dependence between the features of pre-edge C_{1s} *K*-edge absorption spectra for different sizes of the nanodiamond particle with the corresponding CH/CH_2 ratio of surface atoms. Based on the results in Fig. 6, we suggest that the relative number of $CH:CH_2:CH_3$ on the surface will affect the distance between adjacent polar C-H bonds resulting in different charge transfers on the related C and H atoms. This redistribution of atomic charge will affect the electronic environment of core levels of the corresponding C atoms (C_{1s} *K*-edge absorption) that can be detected by XAS measurements. It is worthy to note that in Fig. 6, by putting the number of CH_3 terminations equal to zero, we obtain a linear dependence for CH/CH_2 ratio and also HOMO-LUMO energy gap on the size in agreement with the XAS measurement results.[13]

IV. CONCLUSIONS

In summary, in this paper we investigated structural, vibrational, and electronic properties of the cagelike and spherical H-terminated C nanoparticles of different size. Furthermore, two smallest sizes of Si nanoparticles were also considered where more experimental evidences are available. Although the formation energies of cagelike and spherical nanoparticles are comparable, we obtain a large difference in their mechanical stability after structural relaxation. We reported a large amount of induced positive strain more than 5% in the bulk of elastically softened spherical C and Si particles. This is due to a large surface potential that arises from CH_3 and SiH_3 terminations. Our calculated strain for the elastically stiff nanoparticles (0.6%–3.7%) is in agreement with the strain measurements on the porous Si. Some specific sizes and almost all charge states of these spherical C and Si nanoparticles could not undergo the large induced strains and would dissociate from the central region. The cagelike nanoparticles remain, however, stable after structural relaxation. We attributed this difference between surface stress of cagelike and spherical particles to the difference in presence of the CH_3 and SiH_3 terminations on the surface of the unstable spherical structures.

Our proposed picture explains related reported experimental evidences concerning correlation between the measured strain and H coverage in PS. We also reported correlation between the HOMO-LUMO energy gap and CH/CH_2+CH_3 ratio variations with particle size in agreement with the recently reported experimental evidence about correlation between electronic structure and CH/CH_2 ratio of nanodiamond particles by XAS measurements. The calculated vibrational properties of these nanoparticles support the structural stability results. The smallest vibrational frequencies of the C and Si nanoparticles scale as the inverse of their size and also Si nanoparticles are mechanically softer than their C counterparts. Our calculations indicate that in order to obtain final stability of different semiconductor nanoparticles, the mechanical stability under atomic relaxation plays a large role in comparison with formation energy or thermodynamic stability results. Results also reveal the importance of considering type, geometry, and configuration of the surface terminations to estimate the surface potential and the induced bulk strain. Results can be used to predict the stable structure of spherical C and Si nanoparticles.

*m_heidarisaani@alum.sharif.ir

[1] Jean-Yves Raty, G. Galli, C. Bostedt, Tont W. van Byuren, and Louis J. Terminello, Phys. Rev. Lett. **90**, 037401 (2003).
[2] Jean-Yves Raty and G. Galli, Nature Mater. **2**, 792 (2003).
[3] W. Wilson, P. Szajowski, and L. Brus, Science **262**, 1242 (1993).
[4] G. Medeiros-Ribebeiro *et al.*, Science **279**, 353 (1998).
[5] L. T. Canham, Appl. Phys. Lett. **57**, 1046 (1990).
[6] A. Halimaoui, C. Oules, G. Bomchil, A. Bsiesy, F. Gaspard, R.

Herino, M. Ligeon, and F. Muller, Appl. Phys. Lett. **59**, 304 (1991).
[7] J. E. Dahl, S. G. Liu, and R. M. K. Carlson, Science **299**, 96 (2003).
[8] G. C. McIntosh, M. Yoon, S. Berber, and D. Tomanek, Phys. Rev. B **70**, 045401 (2004).
[9] A. J. Lu, B. C. Pan, and J. G. Han, Phys. Rev. B **72**, 035447 (2005).
[10] N. D. Drummond, A. J. Williamson, R. J. Needs, and G. Galli, Phys. Rev. Lett. **95**, 096801 (2005).
[11] D. Buttard, G. Dolino, C. Faivre, A. Halimaoui, F. Comin, V. Formoso, and L. Ortega, J. Appl. Phys. **85**, 7105 (1999).
[12] M. Heidari Saani, M. Kargarian, and A. Ranjbar, Phys. Rev. B **76**, 035417 (2007).
[13] T. M. Willey, C. BostedtT. van Buuren, J. E. Dahl, S. G. Liu, R. M. K. Carlson, L. J. Terminello, and T. Moller, Phys. Rev. Lett. **95**, 113401 (2005).
[14] M. J. Frisch *et al.*, GAUSSIAN 03, Revision A.7, Gaussian, Inc., Pittsburgh, PA, 1998.
[15] A. D. Becke, J. Chem. Phys. **98**, 5648 (1993).
[16] H.-Ch. Weissker, J. Furthmüller, and F. Bechstedt, Phys. Rev. B **72**, 045351 (2005).
[17] L. E. Ramos, J. Furthmüller, and F. Bechstedt, Phys. Rev. B **72**, 045351 (2005).
[18] K. H. Kim, G. Bai, M. Nicolet, and A. Venezia, J. Appl. Phys. **69**, 2201 (1990).
[19] H. Sugiyama and O. Nittono, J. Cryst. Growth **103**, 156 (1990).
[20] D. Buttard, D. Bllet, and G. Dollino, J. Appl. Phys. **79**, 8060 (1996).
[21] T. Ito, H. Kiyama, T. Yasumatsu, H. Watabe, and A. Hiraki, Physica B (Amsterdam) **170**, 535 (1991).
[22] X. P. Li and D. Vanderbilt, Phys. Rev. Lett. **69**, 2543 (1992).
[23] K. Barla, R. Herino, G. Bomchil, J. C. Pfister, and A. Freund, J. Cryst. Growth **68**, 727 (1984).
[24] I. M. Youmg, M. I. J. Beale, and J. D. Benjamin, Appl. Phys. Lett. **46**, 1133 (1985).
[25] G. Dolino, D. Bellet, and C. Faivre, Phys. Rev. B **54**, 17919 (1996).
[26] S. Takeoda, M. Fujii, S. Hayashi, and Keiichi Yamamoto, Phys. Rev. B **58**, 7921 (1998).
[27] J. P. Wilcoxon, G. A. Samara, and P. N. Provencio, Phys. Rev. B **60**, 2704 (1999).
[28] A. Larre, A. Halimaoui, F. Glowacki, F. Ferrieu, Y. Campidelli, and D. Bensahel, Appl. Phys. Lett. **65**, 1566 (1994).
[29] A. Halimaoui, Y. Campidelli, A. Larre, and D. Bensahel, Phys. Status Solidi B **190**, 35 (1995).
[30] L. E. Friedersdorf, P. C. Searson, S. M. Prokes, O. J. Glembocki, and J. M. Macaulay, Appl. Phys. Lett. **60**, 2285 (1992).
[31] J. M. Ryan, P. R. Wamsley, and K. L. Bray, Appl. Phys. Lett. **63**, 2260 (1993).
[32] B. Welder, C. K. Kim, M. Cardona, and S. Rodriguez, Solid State Commun. **17**, 1021 (1975).
[33] D. Buttard, D. Bellet, and G. Dolino, J. Appl. Phys. **79**, 8060 (1996).
[34] D. Bellet and G. Dollino, Phys. Rev. B **50**, 17162 (1994).
[35] M. V. Wolkin, J. Jorne, P. M. Fauchet, G. Allan, and C. Delerue, Phys. Rev. Lett. **82**, 197 (1999).
[36] I. Vasiliev, J. R. Chelikowsky, and R. M. Martin, Phys. Rev. B **65**, 121302 (2002).